Pergamon

Int. J. Heat Mass Transfer. Vol. 37, No. 8, pp. 1217–1226, 1994

0017-9310/94 $7.00 + 0.00

0017-9310(93)E0037-H

Experimental and numerical studies of evaporating wavy fuel films in turbulent air flow

J. HIMMELSBACH†, B. NOLL‡ and S. WITTIG

Lehrstuhl und Institut für Thermische Strömungsmaschinen, Universität Karlsruhe (T.H.), Kaiserstr. 12, D-76131 Karlsruhe, Germany

(*Received* 2 *June* 1993 *and in final form* 18 *October* 1993)

Abstract—In extending earlier studies the present paper is concerned with the two phase flow inside prefilming airblast atomizers of gas turbine combustors at elevated temperatures. A numerical procedure is presented, which describes the internal flow of the nozzle, with the turbulent air flow and the shear driven evaporating wavy liquid film. The flow conditions of the film and gas at the atomizing edge as well as the pressure drop inside the nozzle are predicted. The theoretical results are compared with detailed measurements of the wavy liquid film and of the gas phase. For the experiments, the test section and the optical measuring techniques for evaporating wavy liquid films presented in a recent paper were employed. Using time-averaged values for the thickness, the velocity and the roughness of the film and assuming laminar film flow, the code leads to accurate predictions of the interaction of the liquid film with the gas phase. A variation of the dominating parameters such as the gas velocity, gas temperature, liquid flow rate, and pressure illustrates the accuracy of the numerical predictions with respect to the gas flow as well as to the film flow. The pressure drop as well as the film temperature, film thickness and velocity are accurately predicted under all conditions. Although the present study is focused on prefilming airblast atomization, the benefits of the calculational procedure are not limited to atomization processes. Quite similar flow conditions are found in intake pipes of internal combustion engines and in film vaporization employing combustors.

INTRODUCTION

FOR PREFILMING airblast atomizers, a large number of detailed data exists on the spray characteristics at low temperatures (e.g. Lefebvre [1], Aigner and Wittig [2, 3], Sattelmayer and Wittig [4, 5], Kneer *et al.* [6]). However, under real operating conditions of combustion chambers in gas turbines the temperature level is much heigher than in most of the experimental investigations. Since the properties of the gas and liquid are strongly varying with temperature, the question arises, how the large base of experimental data at low temperatures can be scaled up to real running coditions of the engine. This problem can be solved with the aid of a calculational procedure for the internal two phase flow with a wavy liquid film inside the nozzle.

At elevated temperatures the two phase flow inside the nozzle is characterized by a coupled momentum, heat and mass transfer within the different phases and the unknown coupling conditions at the liquid/gas interface (Fig. 1). Depending on the flow rates and temperatures of the gas and the liquid, different velocity profiles of the gas phase and of the liquid film are found. In addition, the temperature profiles of the gas and the liquid change locally, as well as the concentration profiles of the vaporized liquid. Special problems appear in the correct description of the coupling conditions for the momentum, the heat and the mass transfer at the phase interface.

For a prediction of the complex multi-phase flow in practical engine design a variety of simplifications is necessary. In the study presented here, suitable simplifications are discussed and examined by a comparison of theoretical results with detailed experiments.

CALCULATIONAL PROCEDURE

It is known from our earlier studies (see in Wittig *et al.* [7]), that a numerical simulation of the two phase flow with wavy liquid film may be based on time-averaged quantities.

In contrast to other applications (e.g. Renz [8], Schultz [9], Shembharkar and Pai [10], Baumann and Thiele [11]) the roughness of the wavy liquid film and the reduction of the effective gap hight by the film thickness must be taken into account in considering the flow inside airblast atomizers.

The calculation of the gas phase flow is based on the Reynolds-averaged Navier–Stokes-equations in connection with equations for energy and species transport. All properties of the gas phase are calculated as functions of temperature, pressure and con-

†Author to whom correspondence concerning this manuscript should be addressed at STE, Zugspitzstraße 80, D-82131 Gauting, München, Germany.

‡ESG, Oliverstraße 10, D-76532 Baden-Baden, Germany.

NOMENCLATURE

C	constant in the logarithmic law of the wall
c_p	specific heat [J kg^{-1} K^{-1}]
c_1	concentration of vapour
h_t	stagnation enthalpy [J kg^{-1}]
$h_{s,0}$	gap height without film [m]
$(h_{1,I}-h_{F,I})$	latent heat of evaporation [J kg^{-1}]
$\dot{H}'_F$	enthalpy flux of the liquid per unit breadth [W m^{-1}]
$\bar{h}_F$	time-averaged film thickness [m]
k_s	equivalent sandgrain roughness [m]
$\dot{m}$	mass flux [kg s^{-1}]
p	pressure [N m^{-2}]
Pr	Prandtl number
$\dot{q}$	heat flux per unit area [W m^{-2}]
Re	Reynolds number
St	Schmidt number
T	temperature [K]
u	gas velocity [m s^{-1}]
u_F	film velocity [m s^{-1}]
u_τ	shear stress velocity [m s^{-1}]
u^+	nondimensional velocity
$\dot{V}_F/B$	liquid volume flux per unit breadth [m^2 s^{-1}]
x	coordinate in axial flow direction [m]
y	coordinate in vertical flow direction [m]
y^+	nondimensional wall distance.

Greek symbols

Δn	normal distance from wall [m]
Δp_{rel}	relative pressure drop
κ'	von Karman constant
λ	thermal conductivity [W m^{-1} K^{-1}]
μ	dynamic viscosity [N s m^{-2}]
ν	kinematic viscosity [m^2 s^{-1}]
ρ	density [kg m^{-3}]
τ	shear stress [N m^{-2}]
ψ_τ	efficiency factor of film roughness.

Subscripts

F	film, liquid
G	gas
I	interface gas liquid
W	wall
P	grid point adjacent to the wall
t	stagnation, turbulent, tangential
1	vapour
0	value at gap entrance.

Superscripts

′	per unit breadth, turbulent variation
″	per unit area.

centration, assuming ideal gas behaviour. In spite of the well known problems associated with the modelling of near wall turbulence, a standard k–ε-turbulence-model is used for the gas phase. Detailed measurements of the surface structure (e.g. Sattelmayer and Wittig [4]) show that the wavyness of the film surface is higher than the laminar sublayer for most of the liquid flow rates. Therefore, more sophisticated turbulence models do not promise significant advantages for the present investigation. Although the elliptic code with bodyfitted coordinates (TEFAC2D, Wittig *et al.* [12], Bauer [13]), which is used in the calculation of the gas phase, would be able to resolve the gas flow near the wavy film surface, this was omitted, because of the extreme numerical effort in modelling moving film waves with wavelengths of 1 mm and less. Thus, near the film surface, modified wall functions based on the well-known logarithmic law of the wall are used. Naturally, this can only be an approximation of the real physical phenomena. However, the results presented in a recent paper (Wittig *et al.* [7]) and the additional results presented here justify this simplification.

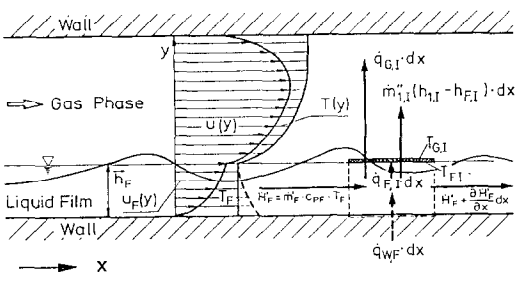

FIG. 1. Two phase flow with evaporating wavy liquid film.

The boundary conditions near the phase interface are described by a sandgrain approach

$$k_s = \psi_\tau \cdot 2 \cdot \bar{h}_F \tag{1}$$

$$\psi_\tau = 0.735 + 0.009255 \cdot \tau_W,$$

where k_s is the sandgrain roughness.

After measuring the boundary layer of the turbulent air over liquid films with various properties characteristic for fuels, and measuring the film thickness at low air temperatures, Sattelmayer and Wittig [4] found this correlation for ψ_τ to give good results for the velocity profile of the gas phase in connection with the logarithmic law of the wall:

$$u^+ = \frac{1}{\kappa'} \ln y^+ + C(Re_{ks}) \tag{2}$$

with:

$$u^+ = \frac{u}{u_\tau} = u\sqrt{\left(\frac{\rho_P}{\tau_W}\right)}$$

$$y^+ = \frac{y u_\tau}{\nu_P}$$

$$Re_{ks} = \frac{u_\tau \cdot k_s}{\nu_P}$$

and with the roughness coefficient $C(Re_{ks})$, which is given by

$$\begin{aligned} C(Re_{ks}) &= 5.15 && Re_{ks} < 5 \\ C(Re_{ks}) &= 1.5497 + 19.1 \cdot \log Re_{ks} \\ &\quad - 14.4339 \cdot (\log Re_{ks})^2 \\ &\quad + 3.30869 \cdot (\log Re_{ks})^3 - \frac{1}{\kappa'} \\ &\quad \cdot \ln Re_{ks} && 5 \leqslant Re_{ks} \leqslant 70 \\ C(Re_{ks}) &= 8.5 - \frac{1}{\kappa'} \cdot \ln Re_{ks} && 70 < Re_{ks}. \end{aligned} \quad (3)$$

Since a variety of different correlations for the description of the roughness can be found in the literature, this correlation for the roughness coefficient proposed by Sattelmayer [14] was compared with functions presented by Cebeci and Bradshaw [15] and values obtained from a study of Ligrani [16]. There are only minor differences between the three correlations. In connection with the standard k–ε–turbulence-model the following wall functions result for the calculation of the momentum transfer in the gas phase.

Shear stress and velocity at the grid point P adjacent to the wall (film surface):

$$\frac{u_{t,P}}{\tau_W/\rho_P} \cdot C_\mu^{0.25} \cdot k_P^{0.5} = \frac{1}{\kappa'} \ln \left(\frac{e^{C(Re_{ks})\kappa'} \cdot \Delta n \cdot C_\mu^{0.25} \cdot k_P^{0.5}}{\nu_P} \right) \quad (4)$$

Turbulent kinetic energy:

$$k_P = \frac{\tau_W/\rho_P}{C_\mu^{0.5}} \quad (5)$$

Dissipation rate:

$$\varepsilon_P = \frac{C_\mu^{0.75} \cdot k_P^{1.5}}{\kappa' \cdot \Delta n}. \quad (6)$$

In this context it has to be mentioned that the above wall functions are not exact for nonisothermal boundaries over evaporating liquids and flows with pressure gradients. In order to reduce effects of the nonisothermal flow with varying local vapour concentration, the grid for the gas phase was optimized to fulfill the condition $y_P^+ = 30 \pm 10$.

To take into account effects of pressure gradients and of the mass flow normal to the film surface, which results from the evaporation, an averaged shear stress calculated from

$$\bar{\tau} = \tau_w + \frac{\dot{m}''_{1W} \cdot u_P}{[1 + ((\tau_w/(\rho \cdot u^2)_P)^{0.5})/\kappa']} + 0.5 \cdot \Delta n \cdot \frac{dp}{dx} \quad (7)$$

was used instead of τ_w in the wall functions ($\tau_w \to \bar{\tau}$). A similar procedure was proposed by Spalding [17].

For the prediction of the heat and mass transfer processes, the well known standard wall functions for the stagnation temperature and the vapour concentration (Spalding [17]) are used. However, as earlier experiments show (Sill [18]), the roughness of the wavy liquid film has only a minor effect on the heat and mass transfer in comparison to the momentum transfer. Therefore, an empirical correlation is used in the numerical code for the gas phase, relating the enhancement of heat transfer by roughened surfaces to the rise of momentum transfer by

$$\eta_{\dot{q}} = \frac{St}{St_o} = \frac{c_f}{c_{f,o}} = \eta_{\dot{q}}(Re_{k_s}, Pr) \quad (8)$$

with

$$\eta_q = \log \left(\frac{Pr^{0.33}}{Re_{k_s}^{0.243}} \right) - 0.32 \times 10^{-3} Re_{k_s} \log (Pr) + 1.225. \quad (9)$$

The above correlation was developed by Burck [19] from heat transfer measurements on roughened surfaces without evaporating liquid and extended by Sill [18] for evaporating water films.

By introducing the stagnation enthalpy, the following formulation of the wall function for the heat transfer with evaporating wavy film surfaces results:

$$St^* = \frac{-\dot{q}_w}{\varrho_P u_{t,P} \left[h_{t,P} - h_{t,W} - (1 - Pr_t) \frac{u_{t,P}^2}{2} \right]} = \frac{\eta_{\dot{q}} c_f^*}{Pr_t (1 + P\sqrt{(\eta_{\dot{q}} c_f^*)})}$$

$$c_f^* = \frac{\bar{\tau}}{\varrho_P u_{t,P}^2}$$

$$P = 9.0 \left(\frac{Pr}{Pr_t} - 1 \right) \left(\frac{Pr_t}{Pr} \right)^{0.25}. \quad (10)$$

The corresponding wall function for the mass transfer

$$St_m^* = \frac{-\dot{m}''_{1,W} (1 - c_{1,W})}{\varrho_P u_{t,P} (c_{1,P} - c_{1,W})} = \frac{\eta_m c_f^*}{Sc_t (1 + P_m \sqrt{(\eta_m c_f^*)})} \quad (11)$$

is obtained from the assumption that the effect of roughness on the mass transfer can be described in similarity to the heat transfer, by replacing the Prandtl-numbers by the Schmidt-numbers.

With the equations given above, the gas flow over evaporating wavy liquid films can be calculated with a limited numerical effort. However, the gas flow is only one aspect of a detailed description of the two phase flow inside a prefilming airblast atomizer or in a combustor employing film vaporization. In the following, a new approach for the mathematical description of the liquid film flow and especially of

the boundary conditions at the phase interface is proposed. *A priori* neither the film thickness or the film velocity distribution are known, nor the film temperatures, the relation between the heat transferred into the liquid film and the latent heat for the evaporation.

As shown in a recent paper (Wittig *et al.* [7]), the film thickness and the velocity in the film can be described in a simple way utilizing time-averaged analytical velocity profiles inside the film. A detailed comparison of the two physical extremes for the time-averaged film velocity profiles was presented for low air temperatures without significant evaporation: a turbulent film velocity profile developed by Wurz [20]

$$u_F^+ = \frac{1}{2\kappa' y_F^+} - \frac{1}{\kappa'}\sqrt{\left(1+\left(\frac{1}{2\kappa' y_F^+}\right)^2\right)} + \frac{1}{\kappa'}\ln\left(2\kappa' y_F^+\left(1+\sqrt{\left(1+\left(\frac{1}{2\kappa' y_F^+}\right)^2\right)}\right)\right) \quad (12)$$

as well as the laminar profile

$$u_F^+ = y_F^+ \quad (13)$$

with:

$$u_F^+ = \frac{u_F}{u_{\tau_i}} = u_F\sqrt{\left(\frac{\rho_F}{\tau_F}\right)}$$

$$y_F^+ = \frac{y_F u_{\tau_F}}{\nu_F}.$$

Both relations are based on the assumption of a constant shear stress over the film thickness. It was found by experiments that the film is showing a laminar rather than a turbulent character in the flow regime, which is of interest here. This new and surprising result was confirmed not only by measurements of the interaction of the film with the gas phase, but also by measurements of the film thickness and film surface velocities for a variety of liquid flow rates and gas velocities.

With the shear stress derived from the calculation of the gas phase and the conservation of mass for the film

$$\int_0^{\delta_F} u_F(y)\,dy = \frac{\dot{m}'_F(x)}{\varrho_F} \quad (14)$$

the local film thickness and velocity can be calculated in a simple way. This information is the base for a detailed calculation of both the liquid and the gas phase, including the heat and mass transfer. It can be used either as a starting condition for a numerical calculation of the gas and the film flow with two almost identical numerical codes for the gas and the film, or in connection with a simpler analytical procedure for the heat and mass transfer within the film. The results presented in this paper show that the simpler second version is already of satisfactory accuracy in many practical engineering problems.

Both calculational procedures are dominated by a balance of heat and mass transfer at the film surface as shown in Fig. 1. The heat of evaporation $\dot{m}''_{i,I}\cdot(h_{i,I}-h_{F,I})\cdot dx$ is determined under the assumption of thermal equilibrium at the phase interface ($T_{F,I} = T_{G,I}$). Thus, the heat transferred from the gas phase

$$\dot{q}_{G,I} = -\varrho\, St^*\, u_{i,P}\left[h_{i,P}-h_{i,I}-(1-Pr_t)\frac{u_{i,P}^2}{2}\right] \quad (15)$$

and the heat transfer inside the film

$$\dot{q}_{F,I} = -\lambda_F\left(\frac{\partial T_F}{\partial y}\right)_I \quad (16)$$

lead to the following equation:

$$\dot{q}_{F,I} - \dot{q}_{G,I} - \dot{m}''_{i,I}(h_{i,I}-h_{F,I}) = 0. \quad (17)$$

EXPERIMENTAL SETUP

The experimental setup with the test section and the optical measuring technique for the film thickness and film surface velocity are described by Wittig *et al.* [7].

The test section (Fig. 2) has a primary cross section of 83×60 mm^2, converging to a cross section of 13×60 mm^2. With the prefilming plate for the liquid film along the centerline of the channel, two gaps of 3.9 mm height are formed. If conditions with heat transfer from the wetted wall to liquid film are chosen, the liquid is only supplied to one side of the plate. Under these conditions the prefilming plate is heated by the flow in the second gap without film. For adiabatic wall conditions, the film is supplied to both sides of the prefilming plate. The test section is designed for a variation of the gas velocities as well as of the pressures and temperatures. Thus the changes of the Reynolds-number of the gas phase by rising the gas temperatures can be compensated by adjusting the pressure in order to get the matching Reynolds-numbers of gas and film for different gas temperatures.

RESULTS

As a first step, measurements at elevated gas temperatures were performed with preheated liquid films ($T_{F,0} = 331$ K), thus providing a nearly homogeneous film temperature throughout the test section. Characteristic results for the gas velocities and temperatures in two measuring planes are given in Figs. 3 and 4 for this test case. The numerical results were obtained with a simplified model for the film ($cp_F \equiv 0$, $\lambda_{F,y} \equiv 0$, $\lambda_{F,y} \equiv \infty$) by assuming an adiabatic prefilming plate. The temperature distribution along the top wall was measured and can be seen from Table 1.

For the gas phase at the inlet a uniform distribution of velocity ($u_{G,0} = 60$ m s^{-1}), temperature ($T_{G,0} = 573$ K), concentration ($c_{i,0} = 0.02$), turbulence level ($Tu = 5\%$) and a turbulent length scale of 5% of the gap height were used. It should be men-

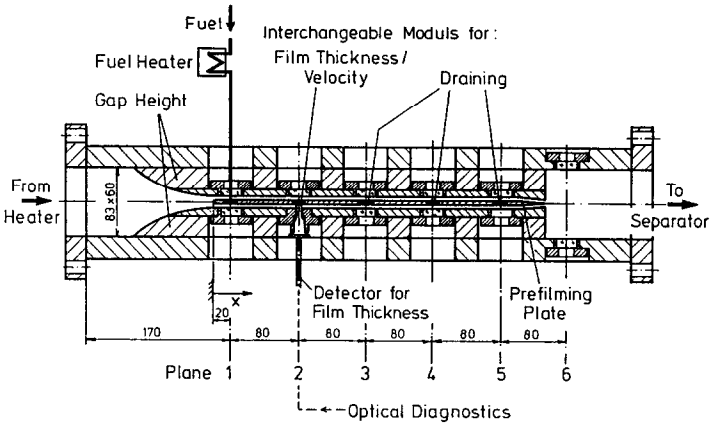

FIG. 2. Test section for evaporating liquid films.

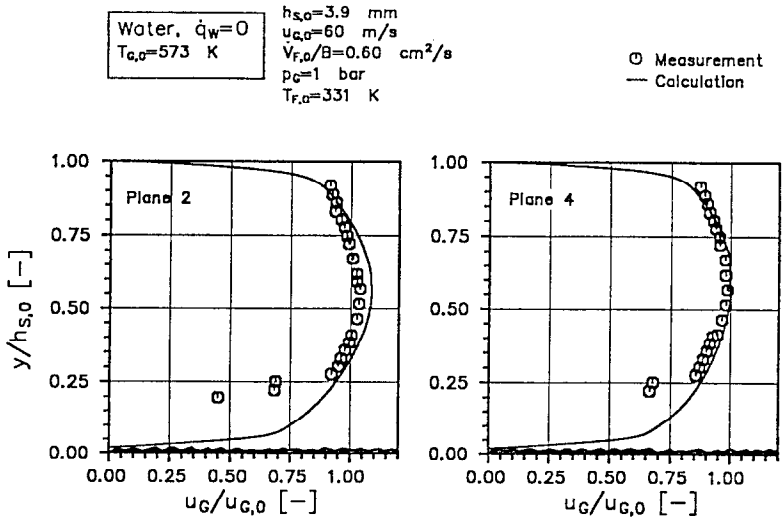

FIG. 3. Measured and calculated gas velocities.

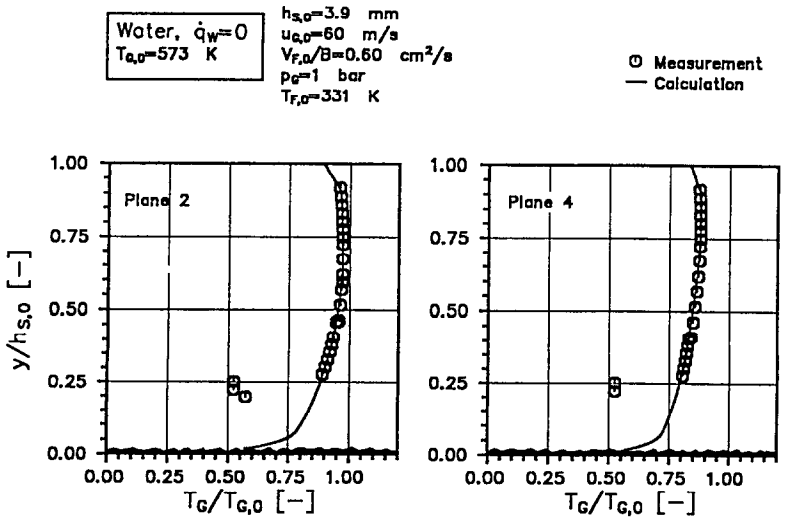

FIG. 4. Measured and calculated gas temperatures.

Table 1. Boundary conditions used in the calculations

No.	$T_{G,0}$ [K]	$u_{G,0}$ [m s^{-1}]	p_G [bar]	$c_{l,0}$ [−]	Temperature at top wall $T = a+bx+cx^2+dx^3$ [K]
1	573	60	1.0	0.020	$0.510601939 \times 10^{3}$ $0.847335076 \times 10^{-1}$ $-0.104370548 \times 10^{-2}$ $0.707471121 \times 10^{-6}$
2	800	60	1.0	0.028	$0.685072024 \times 10^{3}$ $-0.959645657 \times 10^{-1}$ $-0.156279828 \times 10^{-2}$ $0.107428166 \times 10^{-5}$
3	800	150	1.0	0.028	$0.7386012031 \times 10^{3}$ $0.1916057715 \times 10^{0}$ $-0.2617463362 \times 10^{-2}$ $0.3288119619 \times 10^{-5}$
4	800	60	2.5	0.028	$0.7419211133 \times 10^{3}$ $0.1183995651 \times 10^{0}$ $-0.2524659776 \times 10^{-2}$ $0.2735812988 \times 10^{-5}$

tioned that a wire of 0.3 mm diameter was positioned at the upper wall at the gap entrance, in order to avoid effects of laminar–turbulent transition at the top wall, which were not the subject of the present study. On the prefilming plate this was not necessary, as under these conditions the wavyness of the film causes the transition.

The comparison of the measured and calculated gas velocities and temperatures throughout the whole channel shows that the calculational procedure for the gas phase leads to excellent results. The major differences near the wavy film surface (Figs. 3 and 4) are not due to errors from the numerical code. After a detailed analysis it was found that they are caused by liquid fragments impinging on the measuring probe, causing the coupled errors in air temperature, air density and thus also air velocity. The asymmetry in the temperature distribution, caused by the different boundaries with and without film, is predicted as well as the decrease of the gas temperature, which results from the cooling of the gas by the evaporation of the liquid.

Another important point of practical interest is the prediction of the pressure drop inside the gap caused by the roughness effect of the wavy liquid film and by the reduction of the effective gap hight for the gas phase. Experimental and numerical results for the pressure drop

$$\Delta p_{rel} = \frac{p - p(x=0)}{\left(\frac{\rho_G}{2} u_G^2\right) x = 0} \tag{18}$$

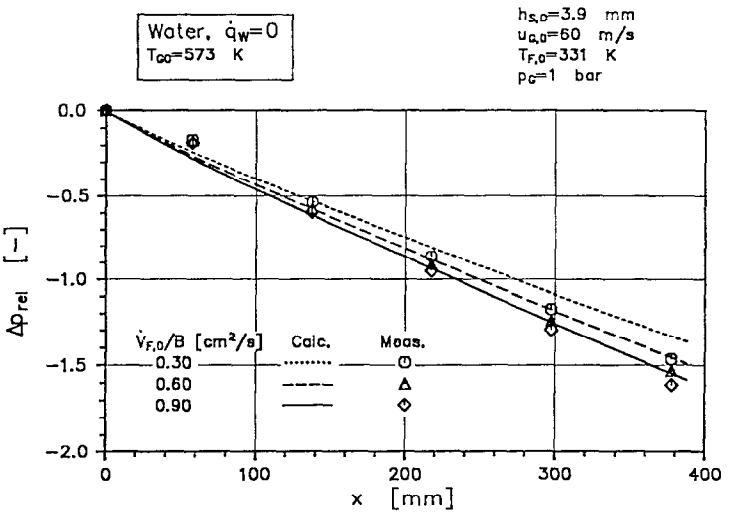

FIG. 5. Pressure drop in the gap.

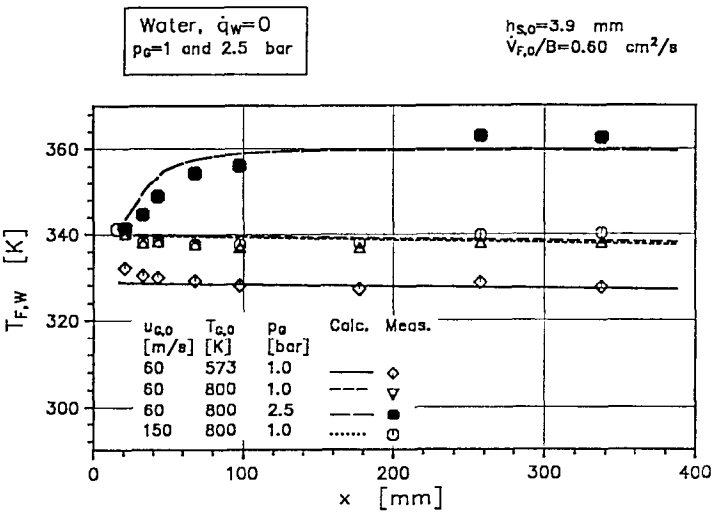

FIG. 6. Film temperatures for different flow conditions (calculation at elevated pressure with finite-volume-codes for film and gas).

from $x = 0$ (see Fig. 2)—where the gap is starting to be parallel—to the other measuring positions within the gap are shown in Fig. 5. Obviously, the pressure drop is well predicted for different liquid flow rates. Similar results were found at elevated gas temperatures and gas velocities, where the evaporation rate of the film is more significant. Naturally, at elevated gas temperatures the film temperatures increased (Fig. 6). In spite of the simplifications of the calculational procedure the predicted film temperatures near equilibrium (preheated film) are confirmed by the measurements.

For predictions under practical engine design conditions the effect of film heating up to equilibrium temperature is of particular interest as well as the effect of increased pressure. Therefore, in Fig. 6 the film temperatures obtained for a gas temperature of $T_{G,0} = 800$ K and a pressure of $p_G = 1$ bar are compared with the data obtained at a pressure of $p_G = 2.5$ bar. At elevated pressures the film temperature is increasing along the prefilming plate, since the properties of the gas and the liquid are strongly dependent on pressure. It has to be emphasized here, that the calculation of the film temperature at elevated pressure was obtained by a detailed numerical analysis of the film with the elliptic finite-volume-code modified for laminar film flow. The results obtained under the assumption of a laminar film flow again indicate that the film shows laminar rather than turbulent characteristics. This observation may be analyzed later on,

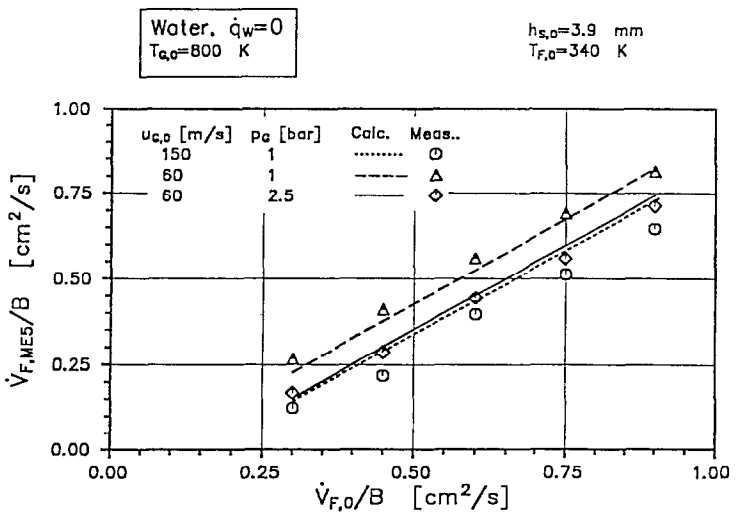

FIG. 7. Liquid flow rates in measuring plane 5 (calculation at elevated pressure with finite-volume-codes for film and gas).

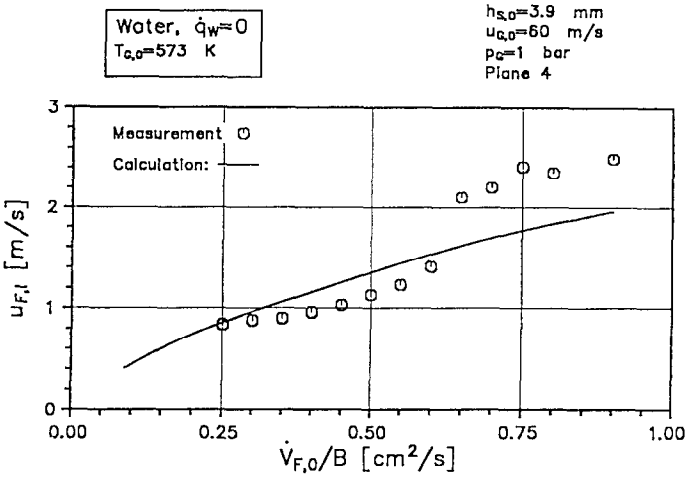

FIG. 8. Film surface velocities.

based on measurements of film thicknesses and velocities.

However, there are some problems for the calculational procedure at high liquid flow rates and at high velocities of the gas phase, which are illustrated in Fig. 7. This figure shows the volume flow rates in measuring plane 5, obtained by draining the liquid. While at lower liquid flow rates the volume rate in plane 5 is computed quite well for all the gas velocities and pressures, there are increasing differences at elevated liquid flow rates. In spite of the well-known inaccuracies of draining procedures (e.g. changes in liquid concentration from evaporation/condensation in the draining system, incomplete draining), these differences—especially at elevated gas velocities—might be caused by droplets torn off the film rather than by mistakes of the measurement. Naturally, these differences cannot be described by the numerical code presented here, but current work is already focussed on that problem. Therefore the optical measuring techniques for film thickness and velocity (Wittig *et al.* [7]) are a valuable tool.

Figure 8 shows an example of the information which can be obtained from measuring the film surface velocities. Here, the same influences as have been obtained by draining the liquid are found. While there are only minor differences at small liquid flow rates, the sudden increase in the measured film velocities is not predicted by the numerical code. The same behaviour occurs at other flow conditions (Wittig *et al.* [7]); however, at different liquid flow rates of course. It results from the instability of the film flow at high liquid flow rates and high shear stresses at the phase interface. In this flow regime the film waves are braking and droplets are torn off the film. These disturbances are moving much faster than the film

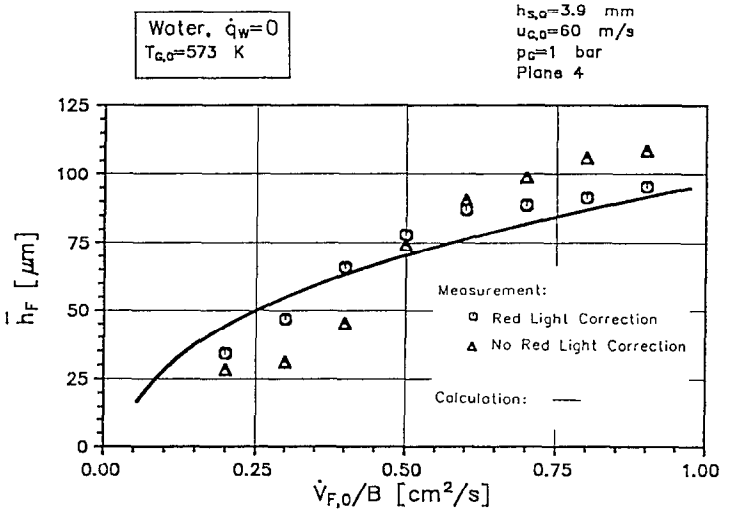

FIG. 9. Film thickness for $T_{G,0}$ = 573 K.

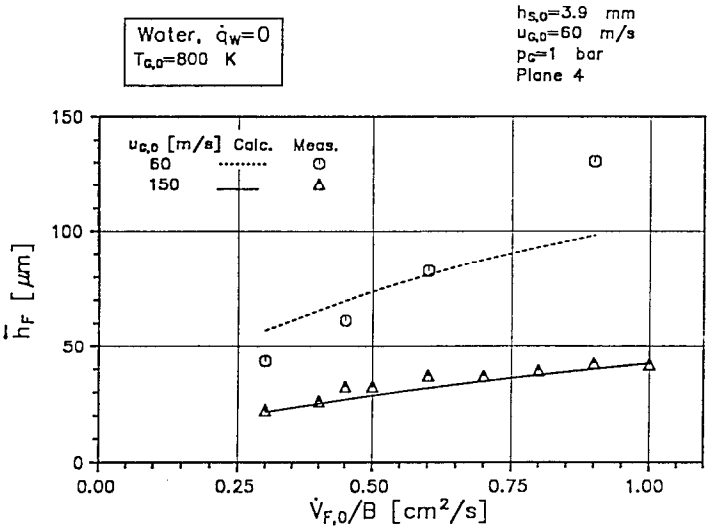

FIG. 10. Film thickness for $T_{G,0} = 800$ K.

and are thus disturbing the measurement. The same disturbances are responsible for the differences in the measured and calculated liquid flow rates in Fig. 7. Comparable measurements at an inlet gas velocity of $u_{G,0} = 150$ m s^{-1} and an inlet gas temperature of $T_{G,0} = 800$ K show that in that flow regime there is already an instability at lower liquid flow rates.

Although the amount of droplets torn off the film is not too high, a small effect can be recognized, when the film temperatures in Fig. 6 are reconsidered. The additional heat and mass transfer caused by the droplets torn off the film produces an elevated vapour concentration in the gas phase, which results in a little increase of the film temperature at the gap exit, and which is not predicted by the numerical code. For the data with the lowest shear stress (1 bar, 60 m s^{-1}) this effect is not recognized.

With exception of the conditions with high liquid flow rates and shear stresses, however, the effects of temperature, pressure, liquid flow rate and gas phase velocity (liquid and gas phase Reynolds-number) on the evaporation process are of good accuracy.

Finally, the film thicknesses presented in Figs. 9 and 10, which were obtained with a two wavelength light absorption technique (Wittig *et al.* [7]) and Himmelsbach [21]), are clearly demonstrating the potential of the code in a large range of flow conditions.

The measuring technique is based on an infrared laser beam, which is absorbed from the liquid, and a superimposed red laser beam, which is not absorbed from the liquid. Thus, potential light intensity losses from light which is reflected from the wavy film surface can be detected with the red laser beam as well as any dirt on the windows and lenses.

For comparison purposes in Fig. 9 the results, as they would have been obtained only with the infrared laser beam without the red light correction, are plotted additionally. Although the variety of effects on the measuring accuracy cannot be displayed in detail here, it can be recognized that the red light correction not only leads to a considerable improvement of the measuring accuracy, but also confirms the above conclusions with respect to the droplets torn off the film. Therefore all the data presented here have been obtained with this technique.

Finally, under consideration of the results for low gas temperatures presented by Wittig *et al.* [7], Himmelsbach [21] and the results presented here, it can be concluded that the two phase flow with wavy liquid film is well predicted in a large range of gas temperatures and flow conditions.

CONCLUSIONS

Turbulent two phase flows with wavy liquid films can be described with acceptable accuracy by employing time-averaged numerical codes. The experimental and numerical results show that, even at high gas velocities, the film shows a laminar rather than a turbulent character as previously assumed by us. The turbulence of the gas phase and the wavyness of the film are not inducing significant turbulence levels into the film. In this context, under conditions with relatively high shear stresses and liquid flow rates, the breaking waves and the droplets torn off the film have been found to be the dominating physical process for heat and mass transfer rather than the onset of turbulence inside the film.

The calculational procedures presented can be incorporated into available numerical codes with a limited effort, in order to predict the flow for numerous other configurations in practical engineering problems with satisfactory accuracy. The velocities, the heat and mass transfer in the film and in the gas phase as well as the pressure drop can be accurately predicted. Restrictions for the application of the

numerical code are limited to extremely high shear stresses and liquid flow rates, where the stability of the film flow is not maintained, and droplets are torn off the film's surface.

Acknowledgement—The present study was supported by a grant from the Sonderforschungsbereich SFB 167 (High Intensity Combustors) of the Deutsche Forschungsgemeinschaft.

REFERENCES

1. A. H. Lefebvre, Airblast atomization, *Prog. Energy Combust. Sci.* **6,** 233–261 (1980).
2. M. Aigner and S. Wittig, Performance and optimization of an airblast nozzle: drop size distribution and volumetric air flow. *Proceedings of the International Conference on Liquid Atomization and Spray Systems*, pp. IIC/3,1–8, London (1985).
3. M. Aigner and S. Wittig, Swirl and counterswirl effects in prefilming airblast atomizers, *Trans.* ASM87-GT-204 (1987).
4. Th. Sattelmayer and S. Wittig, Performance characteristics of prefilming airblast atomizers in comparison with other airblast nozzles. In *Encyclopedia of Fluid Mechanics*, Vol. 8, pp. 1091–1141. Gulf, Houston, TX (1989).
5. Th. Sattelmayer and S. Wittig, Internal flow effects in prefilming airblast atomizers: mechanisms of atomization and droplet spectra, *Trans. ASME* 86-GT-150 (1986).
6. R. Kneer, E. Benz and S. Wittig, Drop motion behind a prefilming airblast atomizer: comparison of phase Doppler measurements with numerical predictions. *Fifth International Symposium on Application of Laser Techniques to Fluid Mechanics*, 9–12 July, Lisbon, Portugal (1990).
7. S. Wittig, J. Himmelsbach, B. Noll, H. J. Feld and W. Samenfink, Motion and evaporation of shear-driven liquid films in turbulent gases. Presented at the Gas Turbine and Aeroengine Congress, Orlando, FL, USA, 3–6 June 1991, *Trans. ASME* 91-GT-207 (1991).
8. U. Renz, Verdunstung mit und ohne Zerfallsreaktionen der Flüssigkeit, Dissertation, Universität Stuttgart, Institut für Thermodynamik der Luft- und Raumfahrt (1971).
9. K.-J. Schultz, Theoretische und experimentelle Untersuchung einer turbulenten ebenen Zweistoffgrenzschicht längs cines verdunstenden Flüssigkeitsfilms, Dissertation, Universität Kaiserslautern (1976).
10. T. R. Shembharkar and B. R. Pai, Prediction of film cooling with liquid coolant, *Int. J. Heat Mass Transfer* **29,** 899–908 (1986).
11. W. W. Baumann and F. Thiele, Heat and mass transfer in evaporating two-component liquid film flow, *Int. J. Heat Mass Transfer* **33,** 267–273 (1990).
12. S. Wittig, H.-J. Bauer and B. Noll, On the application of finite-difference-techniques for the computation of the flow field in gas turbine combustors with complex geometries, AGARD-CP-422 (1987).
13. H.-J. Bauer, Überprüfung numerischer Ansätze zur Beschreibung turbulenter elliptischer Strömungen in komplexen Geometrien mit Hilfe konturangepaßter Koordinaten, Dissertation, Universität Karlsruhe, Institut für Thermische Strömungsmaschinen (1989).
14. Th. Sattelmayer, Zum Einfluß der ausgebildeten, turbulenten Luft-Flüssigkeitsfilm-Strömung auf den Filmzerfall und die Tropfenbildung am Austritt von Spalten geringer Höhe, Dissertation, Universität Karlsruhe, Institut für Thermische Strömungsmaschinen (1985).
15. T. Cebeci and P. Bradshaw, *Momentum Transfer in Boundary Layers*. Hemisphere, Washington, DC (1977).
16. P. M. Ligrani, Structure of turbulent boundary layers. In *Encyclopedia of Fluid Mechanics*, Vol. 8, pp. 111–189. Gulf, Houston, TX (1989).
17. D. B. Spalding, *Genmix—A General Computer Program for Two-Dimensional Parabolic Phenomena*. Pergamon Press, Oxford (1977).
18. K. H. Sill, Wärme- und Stoffübergang in turbulenten Strömungsgrenz schichten längs verdunstender welliger Wasserfilme, Dissertation, Universität Karlsruhe, Institut für Thermische Strömungsmaschinen (1982).
19. E. Burck, Der Einfluß der Prandtlzahl auf den Wärmeübergang und Druckverlust künstlich aufgerauhter Strömungskanäle, *Wärme- und Stoffübertragung* **2,** 87–98 (1969).
20. D. Wurz, Experimentelle Untersuchung des Strömungsverhaltens dünner Wasserfilme und deren Rückwirkung auf einen gleichgerichteten Luftstrom mäßiger bis hoher Unterschallgeschwindigkeit, Dissertation, Universität Karlsruhe, Institut für Thermische Strömungsmaschinen (1971).
21. J. Himmelsbach, Zweiphasenströmungen mit schubspannungsgetriebenen welligen Flüssigkeitsfilmen in turbulenter Heißluftströmung—Meßtechnische Erfassung und numerische Beschreibung, Dissertation, Universität Karlsruhe, Institut für Thermische Strömungsmaschinen (1992).